Carbohydrate Polymers 76 (2009) 381–388

Contents lists available at ScienceDirect

Carbohydrate Polymers

journal homepage: www.elsevier.com/locate/carbpol

Linear modelling of biopolymer systems and related mechanical properties

S. Guessasma *, A. Hamdi, D. Lourdin

INRA, Unite BIA, Rue de la Géraudière, Nantes 44130, France

ARTICLE INFO

Article history:
Received 27 May 2008
Received in revised form 28 October 2008
Accepted 29 October 2008
Available online 7 November 2008

Keywords:
Biopolymer composite
Random microstructure
Monte Carlo
Ising model
Finite element method
Young's modulus

ABSTRACT

A numerical method is proposed to assess the role of random microstructure on the effective Young's modulus of a two-phase biopolymer composite material. An Ising model coupled to a Monte Carlo (MC) technique is used to generate virtual microstructures representing realistic starch–zein blends having random microstructure. The motivation here was to generate virtual microstructures that can be used in a numerical model to allow a continuous variation of both phase fraction and interface length. From the Pair Correlation Function (PCF), the minimum requirement for the Representative Volume Element (RVE) is established based on geometrical considerations. Finite element analysis allowed the prediction of the effective Young's modulus as function of the phase ratio for the studied microstructures. The predicted trend is found close to that of Confocal Laser Scanning Microscopy (CLSM) microstructures of starch-based blends used as a case study. The comparison between the predicted results and the most popular analytical expressions points out that only the Hashin–Shrickman bounds are the most close bounds to the evolution of the effective Young's modulus as function of second phase ratio.

When implementing the intrinsic properties of starch and zein and considering virtual microstructures, analytical and numerical models exhibit the same trend. However, the comparison with the 3-p bending results suggests instead, a non-linear trend that can be inferred to the presence of imperfect starch–zein interface properties.

1. Introduction

Nowadays, bio-based materials are emerging because of their potential use as biodegradable materials to replace fossil-based products such as plastics, packaging components among other applications (Beg, Pickering, & Weal, 2005). As pointed out by several authors, the two main drawbacks for these materials are soft properties, sensitivity to water content and temperature (Gáspár, Benkő, Dogossy, Réczey, & Czigány, 2005). One way to solve these problems is to consider the design of new biopolymer composites under controlled processing conditions as suggested recently (Wu, Sakabe, & Isobe, 2003). By doing so, the compressive yield strength in gluten-based composites can attain, for example, that of polypropylene (Kim, 2008). Despite the large effort that was devoted to the study of biopolymer systems, these studies were almost focusing on kinetics of water sorption, thermomechanical properties and processing routes. Quite a few references are available about the correlation between the effective properties and microstructure features for these materials. As we know, in many practical situations, effective properties of composite materials cannot be approached without considering a large number of structural features inherent to the microstructure details. The most important ones are the volume fraction of the phases, shape descriptors, interface parameters including interface area and inter-phase spacing. Extensive effort has been devoted to relate the effective properties to some microstructural features either by using analytical or numerical approaches.

Generation of multi-inclusion systems was already been explored using different techniques including Monte Carlo, Random Sequential Addition, as well as Simulated Annealing technique (Torquato, 2002).

In this work, the idea of generating virtual microstructures has two main issues:

- obtain a controlled variability in terms of phase ratio and interface quantity in typical biopolymer composite systems;
- predict microstructural features that drive the effective behaviour either by tuning phase or interfacial properties.

Following the original work of Grest and Srolovitz (Grest & Srolovitz, 1984, 1985), two-state microstructures can be generated using Monte Carlo (MC) technique for the study of domain growth kinetics. We demonstrate that this model is able to represent the main structural features attached to real starch–zein microstructures.

* Corresponding author. Tel.: +33 (0) 2 40 67 50 36; fax. +33 (0) 2 40 67 51 67.
E-mail address: sofiane.guessasma@nantes.inra.fr (S. Guessasma).

0144-8617/$ - see front matter © 2008 Elsevier Ltd. All rights reserved.
doi:10.1016/j.carbpol.2008.10.027

The methodology described hereafter assumes the control of both phase ratio and interface length in a two-dimensional grid. Monte Carlo paradigm is used to obtain realistic composite microstructures with random spatial distribution of intrinsic phases. It is a time-saving technique because it determines the final microstructure state giving only an energetic criterion. Thus, no particular requirement for solving state differential equations is needed.

The effective properties of virtual microstructures are computed thanks to the direct import of the generated microstructures into a Finite Element model. The mechanical analysis is performed under linear static elasticity conditions and assuming particular intrinsic properties (the second phase has Young's modulus 10 times larger than that of the matrix). This particular choice of intrinsic parameters has nothing to deal with starch and zein properties but has the merit to provide enough contrast of intrinsic properties. This contrast is required to check that the generated microstructures have similar effective properties to those calculated from real microstructures obtained using confocal microscopy.

Isotropy of the effective properties, or at least the orthotropy, of the virtual microstructures is verified assuming the computation of effective Young's moduli in the two main directions attached to the microstructures. The effective Young's modulus – phase ratio curve is derived and compared to that obtained from real microstructures.

The effective property bounds are determined using various analytical models that are able to describe the elasticity behaviour of two-phase composite materials. Finally, the MC mechanical model is exploited to implement intrinsic properties of zein and starch phases. The predicted result is compared to that issued from threepoint-bending test of starch–zein blends.

2. Modelling techniques

2.1. Microstructure generation technique

In this section, a realistic generation model is suggested to capture the main structural features of starch–zein composites. Obviously, theses systems as those shown later cannot be accurately described using unit-cell models (i.e., one particle embedded in an infinite matrix).

The generation model is built on a two-dimensional microstructure of size $N \times N$. Each square unit (site) has one degree of freedom corresponding to the state (label) that describes the phase nature. The main algorithm steps are illustrated using the flowchart shown in Fig. 1.

These steps can be announced as follows

Step 0: Site labels are randomly distributed in the microstructure. A pseudorandom generator is used to pick out state sequence among the possible phase states. It produces sequences that are uniformly distributed. State (1) corresponds to the matrix phase and state (2) to the second phase. The initial amount of each phase is a control parameter and can be varied to allow different initial microstructures to be generated.

Step 1: A virtual energy of the composite is computed taking into account the intrinsic energy of each phase (core term), the ratio of each phase in the microstructure and the interface energy (interaction term). The energy E of the whole Ising system (i.e., two-state system) represents then the sum of all those terms

$$E = \sum_{i=1}^{N\times N} H_i + \frac{1}{2} J \sum_{i=1}^{N\times N} \sum_{j=1}^{C} (1 - \delta_{ij}) \quad (1)$$

where H is the core energy of a given cluster or domain and it takes two values H_1 and H_2 for the matrix and second phase, respectively. J is an exchange constant $J > 0$. C is the number of nearest neighbours and δ is the kronecker delta.

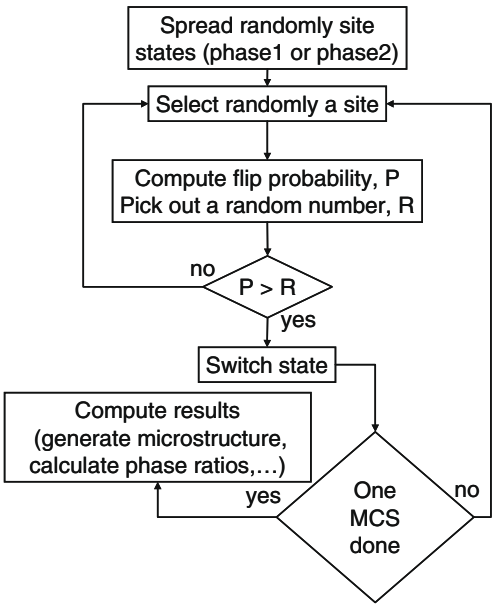

Fig. 1. Monte Carlo algorithm used to generate two-phase microstructures.

Eq. (1) can be rewritten introducing the phase ratios ϕ_1 and ϕ_2 of the matrix and the second phase, respectively

$$E = N \times N(H_1\phi_1 + H_2\phi_2) + \frac{1}{2} J \sum_{i=1}^{N\times N} \sum_{j=1}^{C} (1 - \delta_{ij}) \quad (2)$$

Step2: The ratio and interface quantities are varied by decreasing the system energy (E). The decrease of E is done by considering a Monte Carlo process. Sites are randomly selected individually and flip attempts are performed on each one. The flip is a state switch from matrix to second phase and vice versa. The flip is accepted based on a sigmoid-like probability

$$P = \frac{1}{1 + \exp(\Delta E / kT)} \quad (3)$$

where ΔE represents the change in the energy following the site flip.

Step 3: The flip process is repeated $N \times N$ times. This number scales the unit time in the simulation and is called MCS (Monte Carlo Step). The generation process is stopped after couples of MCSs to obtain the desired phase ratios.

2.2. Finite element calculation

The generated microstructures (image area 512×512 pixels) are implemented in a finite element (FE) code for the calculation of composite effective properties. A two-dimensional plane-stress analysis is assumed. All FE runs are performed using the ANSYS software with a C code that allows the direct import of microstructures. A two-dimensional four-node structural element is used. This element has two degrees of freedom corresponding to the structural displacements UX and UY. The technique considers the conversion of each pixel into the plane element (Fig. 2). Taking into account the real image size of about 200 μm, the pixel size is 0.39 μm. The inputs of the model are Young's moduli of the matrix and second phase, E_1 and E_2, respectively. Poisson ratio is attributed an arbitrary value (0.35) for both phases. A static linear analysis is performed to compute the effective properties in the two perpendicular directions attached to the microstructure as show in Fig. 2. Young's moduli (EX and EY) are calculated as function of phase ratio. The boundary conditions consider a compression

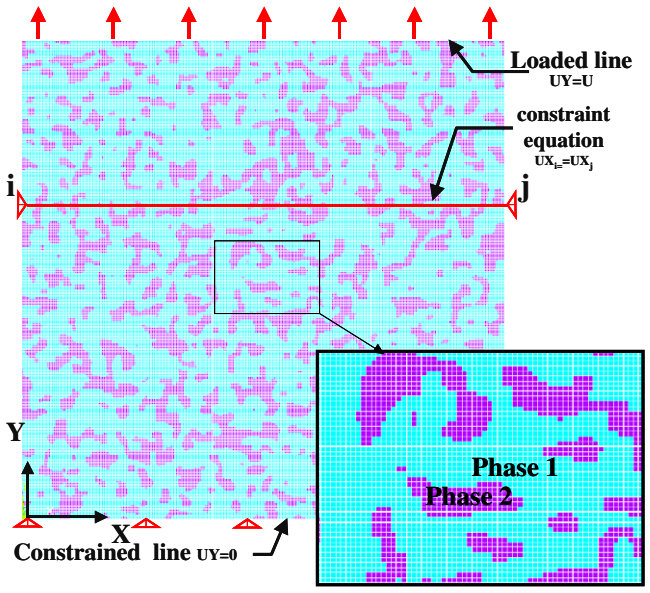

Fig. 2. Boundary conditions considered in the finite element analysis. (For interpretation of the references to colour in this figure legend, the reader is referred to the web version of this article.)

loading conditions. A small displacement is imposed to all nodes belonging to a given line and all nodes of the opposite line are constrained against displacement in the same loading direction (Fig. 2). All nodes of the lateral lines are coupled in a way to allow periodic boundary conditions to be used as illustrated in Fig. 2.

The elastic energy of the FE model is minimised, through an iterative process, using a preconditioned conjugate gradient solver (PCG) for the calculation of the effective properties.

3. Results and discussion

A typical example of the generation process is shown in Fig. 3. The run conditions correspond here to a zero core energy ($H_1 = H_2 = 0$) and a fixed interaction energy ($J = 4$). This condition allows fixing the phase ratio all over the simulation time to nearly the initial value (0.5). It allows also an increase of the domain size of any phase by decreasing the interface length. This decrease is obtained because the energy of the two-phase system (E) is only dependent on the quantity of the interfaces that have to be decreased in the microstructure. The final microstructure at 70 MCS presents a second phase ratio of about 0.53 (Fig. 3e). This ratio compares realistically with typical observed starch–zein microstructures as that shown in Fig. 3d and e. The particle morphology is, in addition, well featured in the simulated microstructure. This point is meaningful and can be inferred to the nature of phase flow during the processing of the biopolymer system. As suggested by the Monte Carlo process, the phase flow can be related to a minimum energy requirement during the material design, which in turn affects the phase morphology. Note that starch–zein microstructure shown in Fig. 3d is obtained using thermomoulding process.

When varying the core energy ratio (H_1/H_2), it is possible to generate microstructures with different particle morphologies and phase ratios. Fig. 4 illustrates this principle for different combinations of matrix initial phase ratio (ϕ_0) and core energies (H_1, H_2).

For a fixed initial ratio ($\phi_0 = 0.3$), the increase of H_2 has the consequence to decrease the second phase domain size. The matrix is more stable from the energy viewpoint ($H_1 < H_2$) as depicted in Fig. 5b. Even if the initial ratio of the matrix is small, ϕ_1 is higher when the ratio H_2/H_1 is large (Fig. 4). When the core energy is set to the ground value, the microstructure evolution depends on the initial phase ratio (ϕ_0) in the following way. If $\phi_0 < 0.5$, the second phase will grow at the expense of the matrix (Fig. 5a) because the matrix particles become instable energetically. Indeed, the ratio interface length/particle area is large in the case of the matrix compared to the second phase. To make this explanation more clear, let's consider disc-like particles. Here, the interface length is proportional to r, where r is the radius of the disc. The ratio interface length/particle area is then proportional to $1/r$. In the same way, when $\phi_0 > 0.5$, the matrix phase is more stable and thus the matrix phase ratio increases with the simulation time accordingly.

3.1. Statistical description of the composite microstructure

If we want that the composite effective properties as computed from the microstructures have some validity at the macroscopic scale, the notion of representative volume element (RVE) is then essential. RVE determines whether the microstructure size is sufficient or not to obtain a stability of the computed properties as function of magnification. Following the standard definition of RVE, two requirements are needed to determine the RVE size: to be sufficiently large for the description of the microstructure heterogeneities and to be much smaller than the macroscopic scale in order use the continuum mechanics theory for the computation of macroscopic properties for any load condition. RVE must be insensitive to particle morphology and boundary conditions used to calculate the effective properties.

Following the work of Chen and co-workers (Chen & Papathanasiou, 2004), the justification of the choice of RVE (representative volume element) can be established if some informative descriptors of the microstructure are used. The second order intensity and the pair correlation (PCF) functions are popular descriptors that can be used for such purpose (Chen & Papathanasiou, 2004). We shall use the PCF function according to the mathematical background detailed in (Mansilla, 2005; Mucharreira, 2000) or recently in (Guessasma, Babin, Della Valle, & Dendievel, 2008). The math describing the PCF is quite simple and leads to the following expression

$$gr = \frac{A}{N^2}\frac{n_{ij}(r)}{2\pi r dr} \tag{4}$$

where $g(r)$ is the PCF depending on the radial distance r. N is the total number of pixels belonging to the second phase in the microstructure. A is the area of the microstructure, thus N/A scales the number density or say, the second phase fraction. $n_{ij}(r)$ is the number of second phase pixels within an annulus of radius r and thickness dr with the centre position at pixel i. Note that Einstein notation is used to represent the sum over all the possible second phase pixels j.

Fig. 6a shows the PCF results for both generated and experimental microstructures of typical biopolymer systems. The real microstructures of starch-based composites are obtained using CLSM (confocal laser scanning microscopy). More information about the processing conditions and image acquisition can be found in (Chanvrier, Della Valle & Lourdin, 2006). We recall here that the PCF quantifies the expectation of a random variable (second phase pixels) in a given region. It represents, in some way, the probability of finding the second phase a given distance away from another possible location. The study of this function is informative about how the second phase pixels pack together. Generally, the function is characterised by a first large peak indicating that, at short distances, the probability of finding a second phase pixel close to a given one is the highest one. At larger distances, the probability of finding pixels with a given separation becomes constant and close to unity.

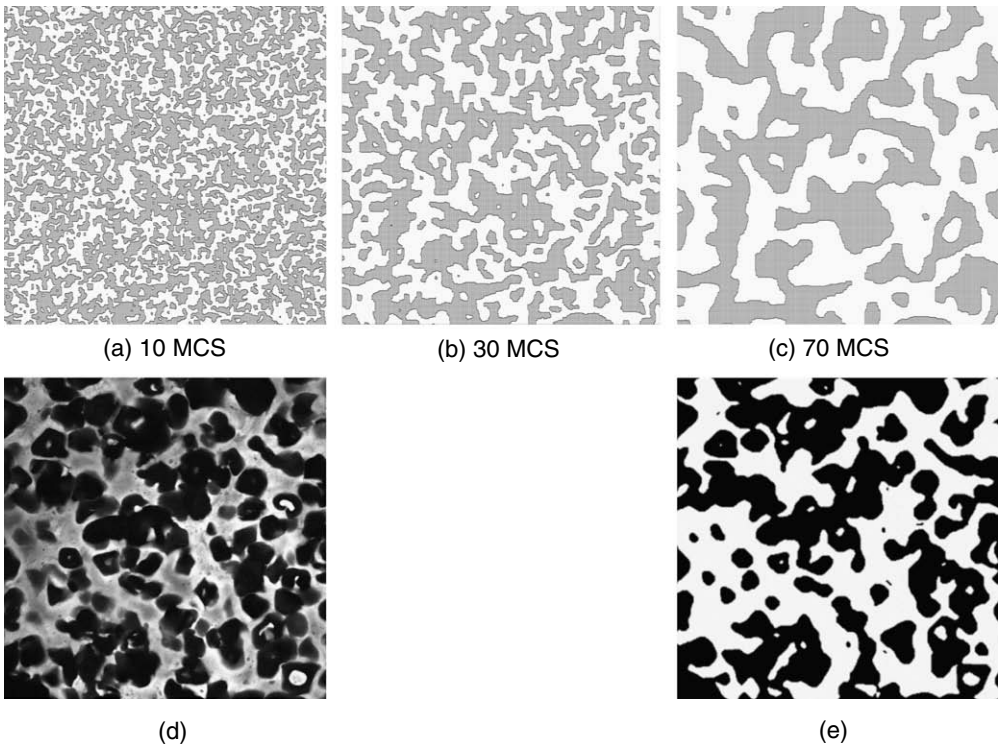

Fig. 3. (a–c) MC microstructure evolution as function of simulation time (512 × 512 pixels). (d) Real microstructure (160 × 160 μm^2) of a biopolymer (starch–zein) composite material of equal phase ratio (starch appears in black). (e) Threshold operation on the real microstructure.

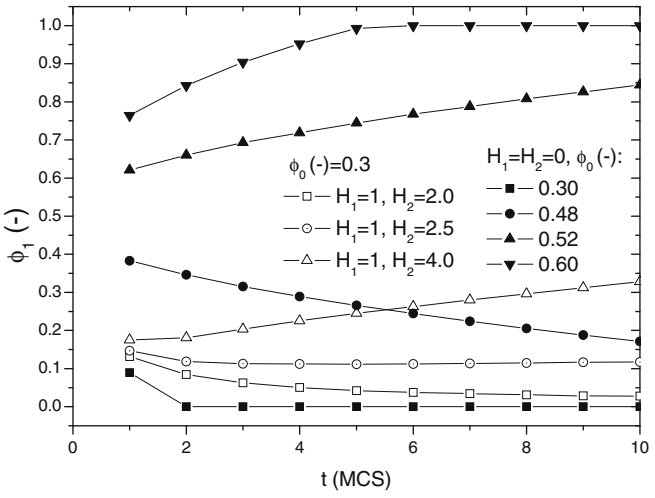

Fig. 4. Ratio of matrix phase (ϕ_1) as function of simulation time for different values of core energies H_1 and H_2 and different initial ratios of the matrix phase (ϕ_0).

Actually, this is a long way of saying that when the PCF vanishes to unity, that distance corresponds to the range of the second phase inter-particle interaction. Thus, if a minimum RVE size has to be chosen, it would be essentially that beyond the interaction range. In our case, the geometrical criterion for the choice of RVE size imposes a lower bound of 30 pixels for the generated microstructures (Fig. 6a). However, for some selected CLSM images, the minimum RVE size depends on the fraction of the second phase in the small fraction range. The model size used for both generated and real microstructures (512 × 512 pixels) is well beyond the minimum required RVE size.

The influence of the element size is also considered through the computation of PCF for pixel sizes ranging from 1 to 10 μm (Fig. 6b). This effect corresponds to the use of different magnifications for a given microstructure. Changing the magnification has to deal with the loose of morphology information. For this particular case, note that the second phase ratio does not evolve significantly (from 0.18 to 0.21) despite the large variation of element size. The evolution of PCF suggests that element size larger than 4 μm cannot guarantee the homogeneity of the microstructure for RVE sizes less than 10 μm. Thus, the effective properties are expected to significantly vary if larger RVE sizes are not used.

3.2. Properties of random microstructures

The sensitivity of the predicted Young's moduli to mesh refinement is studied. Roughly speaking, a fine mesh is generally required to get accurate solutions. For example, the local stress distribution has to be evaluated precisely at the vicinity of the inclusion – matrix interface due to large stress gradients. In the following, the matrix phase is given a larger rigidity (E_1/E_2 = 10) compared to the second phase. The element size is decreased using a mesh factor parameter that expresses the ratio of the element size in the original microstructure over that of the new image. Fig. 7 illustrates typical microstructures with an increasing mesh factor. The loose of main features in the microstructure is clearly highlighted in the smallest grid where the pixel size is 10 μm. In this case, the phase ratio is 5% larger than the original ratio.

The sensitivity of effective Young's modulus to element size is studied as function of simulation time. The run conditions are chosen to allow an increase of the matrix phase ratio. The predicted trend depicted in Fig. 8a reveals an increasing sensitivity of the modulus to mesh coarsening at small simulation times, where the matrix phase ratio (ϕ_1) is near the starting value (ϕ_0 = 0.5). This sensitivity of the effective property is explained by the variation of the phase ratio (ϕ_1) with respect to the element size, which attains in the few first MCS more than 10% (Fig. 8b). Of course, the variation of the phase ratio is due here to a rough approximation of the

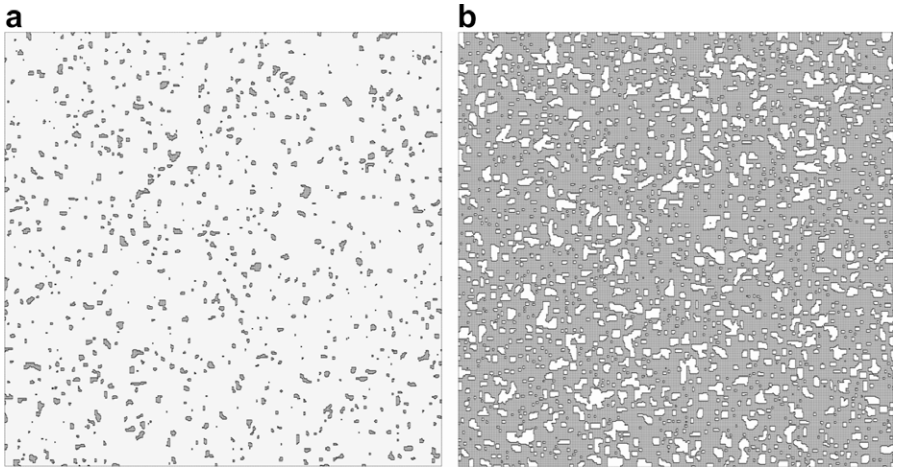

Fig. 5. Examples of simulated microstructures using different combinations of core energies (H_1, H_2) and initial matrix phase ratios ($\phi_{\dot{0}}$). The matrix phase appears in black. (a) $H_1 = H_2 = 0$, $\phi_0 = 0.4$, $t = 4$ MCS, $\phi_1 = 0.95$. (b) $H_1 = 1$, $H_2 = 4$, 0 = 0.3, $t = 6$ MCS, $\phi = 0.26$.

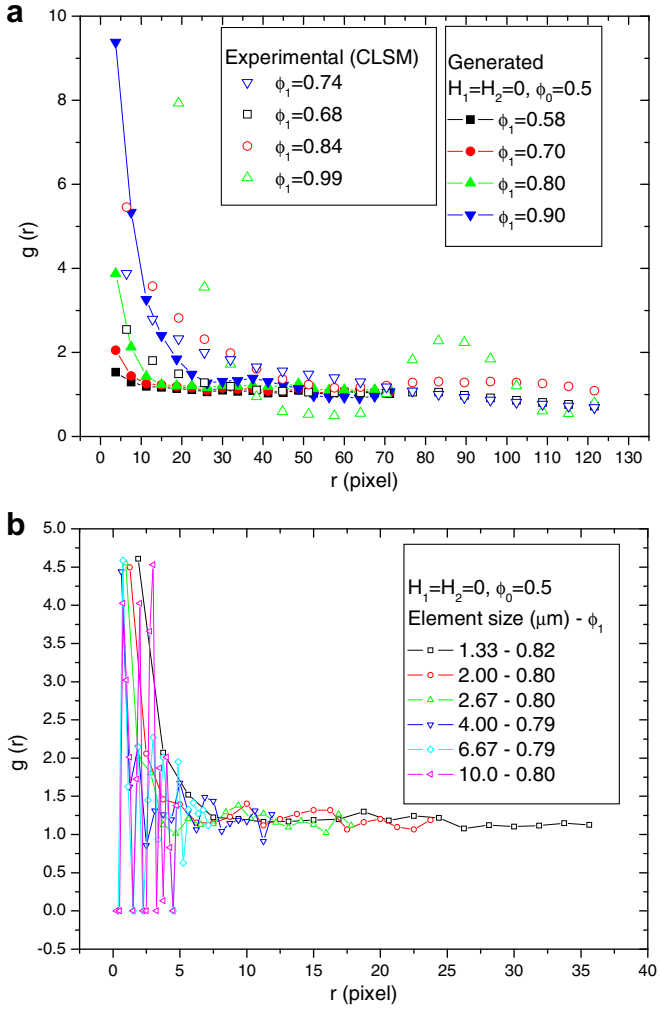

Fig. 6. (a) PCF of generated and real microstructures of biopolymer composites. (b) Effect of element size on PCF profile. (For interpretation of the references to colour in this figure legend, the reader is referred to the web version of this article.)

second phase particle morphology when increasing the element size. This has a consequence to increase the modulus discrepancy especially when the ratio E_1/E_2 is large.

Fig. 8c compares the composite moduli in the X and Y directions. The variation of the modulus as function of studied directions is less than 0.8%. For all studied conditions, the ratio between moduli expressed as EX/EY is equal to 1.01 and determined with a nearly perfect correlation factor ($R^2 = 0.997$). The material is thus orthotropic and we can easily show, based on the random phase distribution in the microstructure, that the composite is isotropic despite that only two directions are considered.

Fig. 9 shows the evolution of the predicted Young's modulus of the composite material (average of EX and EY) as function of second phase ratio. In the same sketch, different bounds are also given based on popular analytical models. These bounds state the envelope in which the composite effective properties should lie irrespective of the phase ratio. Almost models give coherent results at end points ($\phi_1 = 0$ or $\phi_1 = 1$), except for the Eshelby model (Eshelby, 1957). In this model, dilute concentration of the second phase is surrounded by an infinite matrix. The effective properties are given as follows

$$K = K_1 + \frac{\phi_2}{\frac{1}{(K_2 - K_1)} + \frac{3}{3K_1 + 4G_1}} \tag{5}$$

$$G = G_1 + \frac{\phi_2}{\frac{1}{G_2 - G_1} + \frac{6(K_1 + 2G_1)}{5G_1(3K_1 + 4G_1)}} \tag{6}$$

and

$$E = \frac{9KG}{G + 3K} \tag{7}$$

where K, G and E are bulk, shear and Young's moduli, respectively. ϕ_2 is the volume fraction of phase 2.

This model gives a correct estimate of effective Young's modulus if the spacing between inclusions is large. Thus, the model is quite accurate in the small ratio range of second phase. However, it fails in describing the effective property evolution at large ratios as evidently depicted in Fig. 9.

An improvement of Eshelby model is the Mori–Tanaka model (Mori and Tanaka, 1973) which was suggested during the seventieths. The basic idea is to consider the interactions among inhomogeneities. In this model, the overall Young's modulus is only dependent on the phase ratio, aspect ratio and elastic constants of the two phases. Thus, it introduces more information about microstructure features compared to Eshelby model. The stiffness tensor of the composite can be derived as follows (Mori and Tanaka, 1973; Wang & Pyrz, 2004)

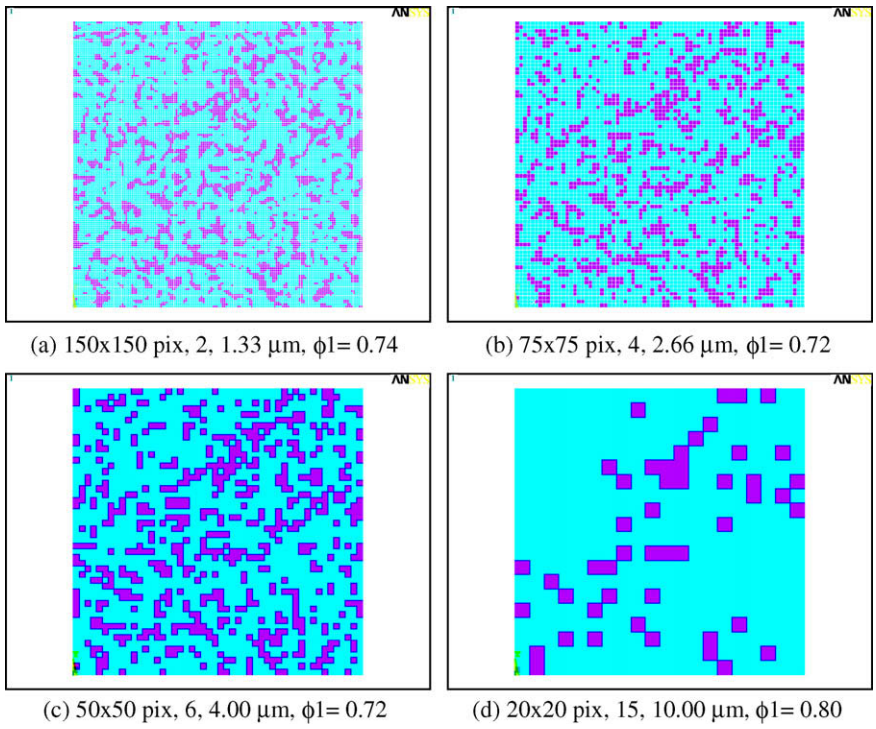

Fig. 7. Typical meshed microstructures with an increased element size. The run parameters are the microstructure size, the element size, the mesh factor and the matrix phase ratio, respectively. The generation parameters are: $t = 8$ MCS, $H_1 = 0$, $H_2 = 0$, $\phi_0 = 0.5$. (For interpretation of the references to colour in this figure legend, the reader is referred to the web version of this article.)

$$L = L_1 + \sum_{i=2}^{N} \phi_i \{(L_i - L_1)T_i\} \left[\sum_{i=2}^{N} \phi_i \{T_i\}\right]^{-1} \tag{8}$$

and

$$T_i = [I + S_i L_1^{-1}(L_i - L_1)]^{-1} \tag{9}$$

where L, L_1 and L_i are the Mori–Tanaka stiffness tensor of the composite, matrix and discrete inhomogeneities labelled by i. ϕ_i is the related volume fraction. Curly brackets denote the average over all possible orientations. S_i is the Eshelby tensor. I is the unit tensor.

The effective properties calculated from the above expression depend on the shape of inhomogeneities as shown by different authors (Shjødt-Thomsen & Pyrz, 2001; Wang & Pyrz, 2004). In the case of a two-phase system, the above expression reduces to (Shjødt-Thomsen & Pyrz, 2001; Wang & Pyrz, 2004)

$$L = L_1 + f_2\{(L_2 - L_1)T_2\}[f_1 I + f_2\{T_2\}]^{-1} \tag{10}$$

In the case of isotropic platelet inclusions, the effective properties are given as follows

$$K = K_1 + \frac{f_2(K_2 - K_1)(3K_1 + 4G_1)}{f_1(K_2 - K_1) + (3K_2 + 4G_1)} \tag{11}$$

$$G = G_1 + \frac{f_2(G_2 - G_1)G_1}{f_1(G_2 - G_1)\frac{6(K_1+2G_1)}{5(3K_1+4G_1)} + G_1} \tag{12}$$

Despite that Mori–Tanaka model is representative of various composite materials effective properties including random and fully oriented reinforcing phase, in our case, this model gives an underestimation of the effective Young's modulus.

The Hashin–Shtrikman model gives the upper and lower bounds in which the effective properties should lie irrespective of any microstructure arrangement (Hashin & Shtrikman, 1963). The variational principle used there holds for a macroscopically homogeneous and isotropic effective properties. The bounds are explicitly function of volume fractions of individual phases and can be announced as follows

$$K^- \leqslant K \leqslant K^+ \tag{13}$$

and

$$G^- \leqslant G \leqslant G^+ \tag{14}$$

where

$$K^- = K_1 + \frac{f_2}{\frac{1}{K_2 - K_1} + \frac{3f_1}{3K_1 + G_1}} \tag{15}$$

and

$$K^+ = K_2 + \frac{f_1}{\frac{1}{K_1 - K_2} + \frac{3f_2}{3K_2 + G_2}} \tag{16}$$

These bounds are given for a matrix phase more compliant than the second phase ($K_2 > K_1$ and $G_2 > G_1$).

As shown in Fig. 9, the composite effective behaviour is quite within the Hashin–Shtrikman bounds. It is also verified that the Hashin–Shtrikman lower bound is coincident with the Mori–Tanaka model in the case of hard isotropic-in-shape inclusions. Another commonly admitted result is that Hashin–Shtrikman bounds are narrower compared to the bounds given by the equal strain (Voight) and equal stress (Reuss) composite model. These last ones correspond to special geometrical combinations of the two phases and can be written as

$$E_R \leqslant E \leqslant E_V \tag{17}$$

where

$$\frac{1}{E_R} = \frac{\phi_1}{E_1} + \frac{\phi_2}{E_2} \tag{18}$$

and

$$E_V = \phi_1 E_1 + \phi_2 E_2 \tag{19}$$

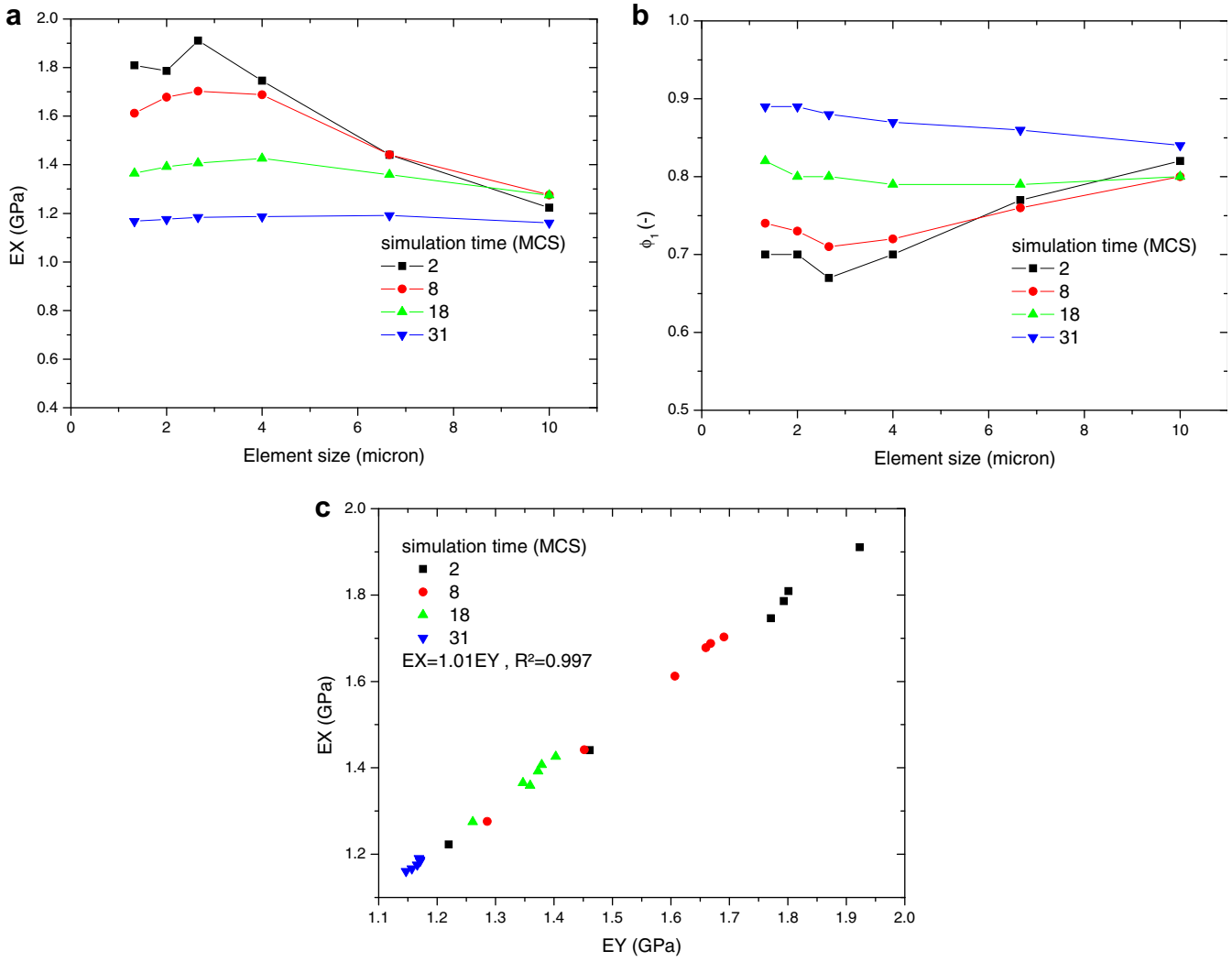

Fig. 8. (a) Evolution of (a) Young's modulus in the *X* direction, (b) Matrix phase ratio (ϕ_1) as function of element size for different simulation times. (c) Young's modulus in the *X* direction as function of that in the *Y* direction for all studied conditions. (For interpretation of the references to colour in this figure legend, the reader is referred to the web version of this article.).

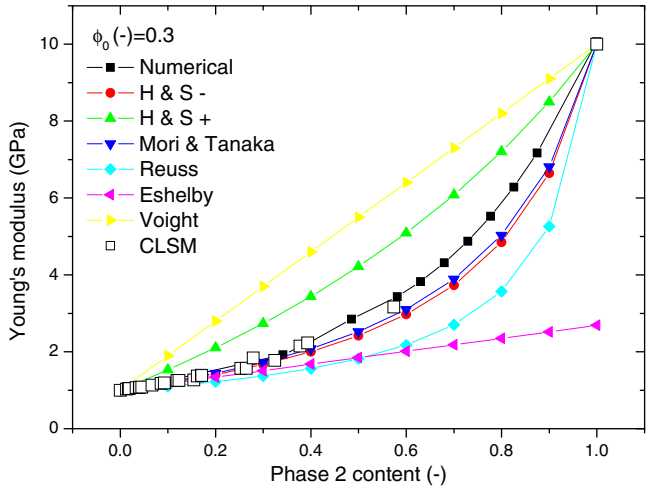

Fig. 9. Predicted effective Young's modulus of the biopolymer composite compared to major theories giving the composite property bounds. (For interpretation of the references to colour in this figure legend, the reader is referred to the web version of this article.)

3.3. Application to real microstructures

The case of real microstructures of starch–zein blends is considered in the following. Images from confocal laser scanning microscopy (CSLM) are meshed using the same scheme as described above (Fig. 10). The physical properties of intrinsic materials are derived from 3p-bending experiments (Chanvrier et al., 2006). Young's moduli of the two phases are quite close (EZ = 3 GPa, ES = 2.62 GPa, where Z and S hold for zein and starch, respectively). In Fig. 11 is depicted the comparison between the experimental, numerical (Finite Element) and analytical models describing the effective Young's modulus of the composite as function of zein content. All analytical and FE models give the same linear result because the intrinsic moduli are merely close.

The variability of the experimental flexural moduli is about 12%. Despite this variability, the experimental results well show that the numerical and analytical models do not explain totally the experimental trend. One major reason explaining this discrepancy would be the imperfect interface properties. Indeed, a recent study (Guessasma, Sehaki, Lourdin, & Bourmaud, in press) has shown that, in the same composite material, the mechanical properties determined using nanoindentation decrease when the indents are performed near the interface. Thus, the presence of an imper-

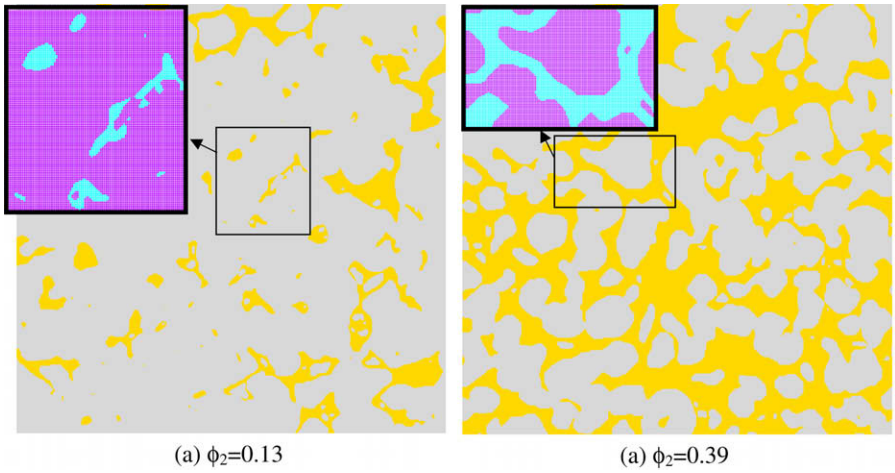

Fig. 10. Meshed CLSM images ($160 \times 160\ \mu m^2$) of starch–zein composites for different zein content. Composites are obtained using a thermomoulding process. (For interpretation of the references to colour in this figure legend, the reader is referred to the web version of this article.)

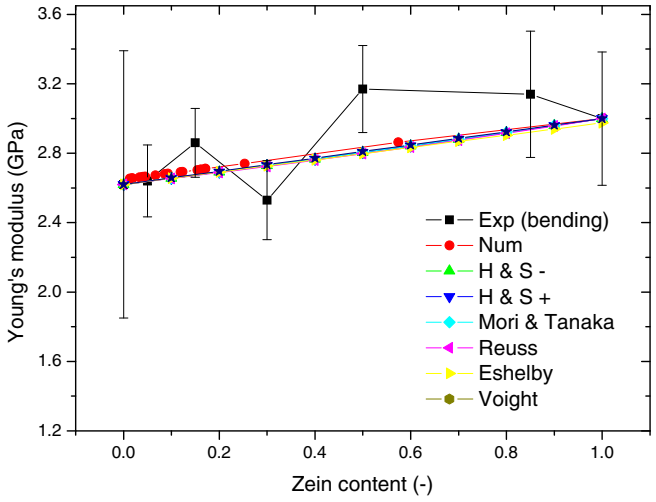

Fig. 11. Comparison between experimental, numerical and analytical approaches to determine the effective properties of the biopolymer composite as function of zein content. (For interpretation of the references to colour in this figure legend, the reader is referred to the web version of this article.)

fect interface will alter the stress transfer between the biopolymer phases and causes the non-linear trend observed in Fig. 11.

4. Concluding remarks

Generation of two-dimensional microstructures using Monte Carlo technique is a realistic model representing the main structural features of biopolymer composites. The calculus of effective properties shows that the Hashin–Shtrikman model has the merit to describe the effective bounds of starch–zein system. Some other analytical models (self-consistent, Mori–Tanaka, Eshelby) lead to either a rough estimate of the bounds or exact solution only in the dilute regime (small second phase fraction).

Giving the experimental values of the starch–zein composite intrinsic parameters, it is found that the effective properties cannot be explained using both numerical and analytical models. This discrepancy is thought, if we exclude experimental variability, to imperfect starch–zein interface properties. As part of another study, handling interface properties in the model requires the implementation of non-linear behaviour at the interface where stress transfer is altered.

References

Beg, M. D. H., Pickering, K. L., & Weal, S. J. (2005). Corn gluten meal as a biodegradable matrix material in wood fibre reinforced composites. *Materials Science and Engineering: A, 412*(1–2), 7–11.

Chanvrier, H., Della Valle, G., & Lourdin, D. (2006). Mechanical behaviour of corn flour and starch–zein based materials in the glassy state: A matrix-particle interpretation. *Carbohydrate Polymers, 65*(3), 346–356.

Chen, X., & Papathanasiou, T. (2004). Interface stress distributions in transversely loaded continuous fiber composites: Parallel computation in multi-fiber RVEs using the boundary element method. *Composites Science and Technology, 64*, 1101–1114.

Eshelby, J. (1957). The determination of the elastic field of an ellipsoidal inclusion. *Proceedings of the Royal Society, A241*, 376–396.

Gáspár, M., Benkő, Z., Dogossy, G., Réczey, K., & Czigány, T. (2005). Reducing water absorption in compostable starch-based plastics. *Polymer Degradation and Stability, 90*(3), 563–569.

Grest, G., & Srolovitz, D. J. (1984). Structure and evolution of quenched Ising clusters. *Physical Review B, 30*(9), 5150–5155.

Grest, G., & Srolovitz, D. J. (1985). Impurity effects on domain-growth kinetics. I. Ising model. *Physical Review B, 32*(5), 3014–3020.

Guessasma, S., Babin, P., Della Valle, G., & Dendievel, R. (2008). Relating cellular structure of open solid food foams to their Young's modulus: Finite element calculation. *International Journal of Solids and Structures, 45*(10), 2881–2896.

Guessasma, S., Sehaki, M., Lourdin, D., & Bourmaud, A. (in press). Viscoelasticity properties of biopolymer composite materials determined using finite element calculation and nanoindentation. *Computational Materials Science*.

Hashin, Z., & Shtrikman, S. (1963). A variational approach to the theory of the elastic behavior of multiphase materials. *Journal of the Mechanics and Physics of Solids, 11*, 127–140.

Kim, S. (2008). Processing and properties of gluten/zein composite. *Bioresource Technology, 99*(6), 2032–2036.

Mansilla, D. (2005). Analysis and simulation of transverse random fracture of long fibre reinforced composites. *EMCI Enginyeria mecànica i de la construcció industrial* (p. 274): Giroda.

Mori, T., & Tanaka, K. (1973). Average stress in matrix and average elastic energy of materials with misfitting inclusions. *Acta Metallurgica, 21*, 571–574.

Mucharreira, S. (2000). Statistical Analysis of Particle Distributions in Composite Materials. *Department of Probability and Statistics* (p. 328): University of Sheffield.

Shjødt-Thomsen, J., & Pyrz, R. (2001). The Mori–Tanaka stiffness tensor: Diagonal symmetry, complex fibre orientations and non-dilute volume fractions. *Mechanics of Materials, 33*, 531–544.

Torquato, S. (2002). Random heterogeneous materials. *Interdisciplinary applied mathematics* (p. 701). Berlin: Springer.

Wang, J., & Pyrz, R. (2004). Prediction of the overall moduli of layered silicate-reinforced nanocomposites – Part I: Basic theory and formulas. *Composites Science and Technology, 64*, 925–934.

Wu, Q. X., Sakabe, H., & Isobe, S. (2003). Processing and properties of low cost corn gluten meal/wood fiber composite. *Industrial & Engineering Chemistry Research, 42*(26), 6765–6773.